DALTON
FULL PAPER

Static and dynamic structures of $CD_3ND_3GeCl_3$ studied by TOF high resolution neutron powder diffraction and solid state NMR

Koji Yamada,*[a] Keiko Mikawa,[a] Tsutomu Okuda[a] and Kevin S. Knight[b]

[a] *Department of Chemistry, Graduate School of Science, Hiroshima University, Kagamiyama 1-3, 739-8526 Higashi-Hiroshima, Japan. E-mail: kyamada@sci.hiroshima-u.ac.jp*
[b] *The Rutherford Appleton Laboratory, Chilton, Didcot, Oxon, UK OX11 0QX. E-mail: K.S.Knight@rl.ac.uk*

Received 31st July 2001, Accepted 13th February 2002
First published as an Advance Article on the web 19th April 2002

$CD_3ND_3GeCl_3$ has been studied by high-resolution neutron powder diffraction and ^2H NMR investigation over a wide temperature range to understand the static and dynamic structures and successive phase transitions. A monoclinic crystal of $CD_3ND_3GeCl_3$ (Phase IV, space group $P2_1/n$) undergoes a phase transition to an orthorhombic system (Phase III, *Pnma*) at 203 K where the symmetry of the anionic sublattice and the geometry of the N–D ··· Cl hydrogen bonds change. Furthermore, Phase III undergoes a phase transition to a trigonal system (Phase II, $R3m$) at 349 K where an orientational disorder of the cation is excited. Our ^{35}Cl NQR measurement also suggested an onset of the reorientation of the pyramidal $GeCl_3^-$ anion just below the phase transition to Phase II with an activation energy $E_a = 60.5$ kJ mol^{-1}. However, a transition from Phase II to a cubic phase (Phase I, $Pm3m$), which was reported to be 396 K on the $CH_3NH_3GeCl_3$, was not complete by 475 K. The Rietveld analysis at 475 K suggested that only 7% of the sample transformed to a cubic perovskite structure in which not only orientational disorder of the cation but also positional disorder of the chloride ion were confirmed, similar to $CH_3NH_3GeCl_3$.

Introduction

Perovskite halides (ABX_3) of group 14 elements such as Ge, Sn and Pb have been studied extensively, partly because of their successive phase transitions and partly because of the diversity of their electrical properties such as ferroelectricity, ionic conductivity and electronic conductivity. The low oxidation state of group 14 elements has an s-electron lone pair and this is the main origin of the interesting structural and electrical properties. According to previous studies, the following general tendencies have been drawn: (1) each BX_6 octahedron tends to deform with decreasing atomic number of the B atom and results in the appearance of an isolated pyramidal BX_3^- anion [1–8] and (2) electronic conductivity appears in bromides or iodides if the distortion from an ideal perovskite is small and the conductivity depends strongly on the lattice constant.[9–13] Furthermore, a ferroelectric property of $CsGeCl_3$ and an antiferroelectric property of $(CH_3)_4NGeCl_3$ were reported.[3,14] The structural tendencies that appear in this perovskite family are closely related to the hypervalent nature of the central metal,[15] that is, a symmetric *trans* X–B–X bond known as a three-center four-electron bond (3c–4e)[16] tends to deform to an asymmetric X–B ··· X bond with decreasing atomic number of the B metal. Similar behavior was reported with decreasing temperature for $CH_3NH_3SnBr_3$, where a red semiconducting cubic crystal undergoes a phase transition to an yellow insulator below 229 K accompanied by a distortion of the perovskite lattice.[4,11] Another example of the phase transition having a hypervalent bond has been recently reported for $(C_5N_5NH)SbBr_4$, in which one symmetric *trans* Br–Sb–Br bond deforms to an asymmetric bond Br–Sb ··· Br^- below 253 K forming an N–H ··· Br hydrogen bond.[17]

In our previous papers we reported successive phase transitions and ionic conductivities for $AGeX_3$ (A = alkylammonium, X = Cl and Br). Among these complexes, $CH_3NH_3GeCl_3$, $(CH_3)_4NGeCl_3$, and $(CH_3)_4NGeBr_3$ showed phase transitions to cubic perovskite structures in which each halide ion occupies the 6*f* site with an occupation factor of 50% instead of the original 3*c* site.[18–20] A dynamical bond switching between Ge–X ··· Ge and Ge ··· X–Ge is excited in the cubic phase and this dynamic property is an interesting phenomenon because it strongly reflects the nature of the hypervalent bond. Furthermore, high ionic conductivity due to halide ions was observed in the cubic phase. In this paper the static and dynamic structures of $CD_3ND_3GeCl_3$ were investigated over a wide temperature range by means of high-resolution neutron powder diffraction and ^2H NMR. An isotope effect upon deuteration was also examined in detail.

Experimental

Preparation of samples

$CH_3NH_3GeCl_3$ was prepared according to the procedure described before.[18] Deuterated compound $CD_3ND_3GeCl_3$ was crystallized from a 6 M DCl (Isotec, 99.8 atom% of D) solution containing equimolar amounts of CD_3ND_3Cl (Isotec, 99.8%) and deuterated germanium(II) hydroxide, $Ge(OD)_2$. $Ge(OD)_2$ was synthesized in advance from $Ge(OH)_2$ by an exchange reaction in an acidic D_2O solution. The crystalline product $CD_3ND_3GeCl_3$ was filtered off and dried *in vacuo*. The crystalline product was characterized by X-ray diffraction followed by a Rietveld analysis. The refined lattice constants are a = 11.206(1) Å, b = 7.427(1) Å, and c = 8.296(1) Å at 294 K and a slight expansion of the lattice was observed compared with the hydrated analog, a = 11.194(1), b = 7.417(1), and c = 8.292(1) Å at 298 K.[19] The deuteration level determined by the broad-line ^1H NMR measurement was 92%.

TOF neutron diffraction

Neutron powder diffraction data were collected at the ISIS neutron spallation source using the high-resolution powder diffractometer, HRPD. Data were recorded at the back-scattering

 DOI: 10.1039/b201611g

This journal is © The Royal Society of Chemistry 2002

detector using two time-of-flight windows, 42–130 and 125–210 ms, which correspond to the *d*-spacing ranges of 0.83–2.57 Å and 2.5–4.15 Å, respectively. Approximately 4.3 g of powder, contained in a thin-walled cylindrical vanadium can with internal diameter 11 mm, were used. Measurements were performed at five different temperatures, 2 K, 150 K, 250 K, 370 K and 475 K. Each raw data set was then normalized to the incident monitor spectrum and background subtracted using programs available at the ISIS. Rietveld refinements were performed using the GSAS program package available from the Los Alamos National Laboratory.[21]

NMR measurement

A homebuilt pulsed spectrometer operating at 6.4 T was used for ^{2}H and ^{14}N NMR with corresponding Larmor frequencies 41.637 MHz and 19.595 MHz, respectively. A conventional quadrupole echo pulse sequence (90–90_{90}-echo) followed by a Fourier transformation was used for ^{2}H NMR. The 90° pulse length was 3 μs for ^{2}H NMR. A single pulse sequence was applied for ^{14}N NMR and 1024 free induction signals were accumulated to get a satisfactory spectrum.

Ionic conductivity

The electrical conductivity was determined by a complex impedance method in the frequency range from 100 Hz to 100 kHz using a pressed pellet coated with carbon electrodes.

Results and discussion

Phase diagrams of $CH_3NH_3GeCl_3$ and $CD_3ND_3GeCl_3$

In order to clarify the relationship between the phases and successive phase transitions, phase diagrams were deduced from DTA, XRD, ^{35}Cl NQR and ^{2}H, ^{14}N NMR measurements as shown in Fig. 1. Each phase is abbreviated as Phase I, II, III,

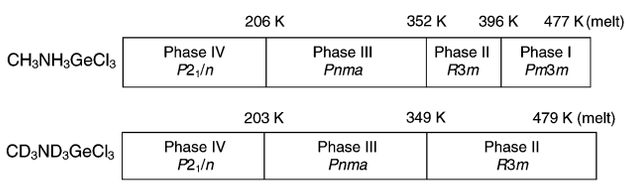

Fig. 1 Phase diagrams for $CH_3NH_3GeCl_3$ and $CD_3ND_3GeCl_3$. The neutron diffraction measurement of $CD_3ND_3GeCl_3$ suggested that 7% of the sample transformed to the cubic phase at 475 K. However, this phase transition did not finish during the measurement.

and IV from the high temperature side according to $CH_3NH_3GeCl_3$. The phase transition temperature from Phase IV to III was determined by the temperature dependence of the ^{35}Cl NQR spectrum and the temperature was also confirmed by the DTA measurement. Fig. 2 plots ^{35}Cl NQR frequencies of $CD_3ND_3GeCl_3$ against temperature. At 77 K three ^{35}Cl NQR signals were observed at 13.550, 12.798 and 12.270 MHz for $CD_3ND_3GeCl_3$ and the corresponding shifts due to the deuteration were −7, −3, and 1 kHz, respectively. There are three crystallographically different Cl sites at Phase IV. With increasing temperature these NQR signals change their frequencies continuously and decrease to two signals at 203 K with an intensity ratio 1 : 2, suggesting the appearance of mirror symmetry (*m*) on the pyramidal $GeCl_3^-$ anion. With further increasing temperature these two NQR signals disappeared just below T_{tr} (Phase III ↔ II) accompanied by a steep decrease of the relaxation time due to the onset of reorientation of the $GeCl_3^-$ anion. We will discuss later this dynamic property of the $GeCl_3^-$ anion by means of NQR T_1 measurements. On the other hand, the ^{2}H NMR quadrupole splitting decreased drastically from *ca.* 40 kHz to 2 kHz at T_{tr} (Phase III ↔ II) as shown in Fig 3. This change suggests the appearance of an

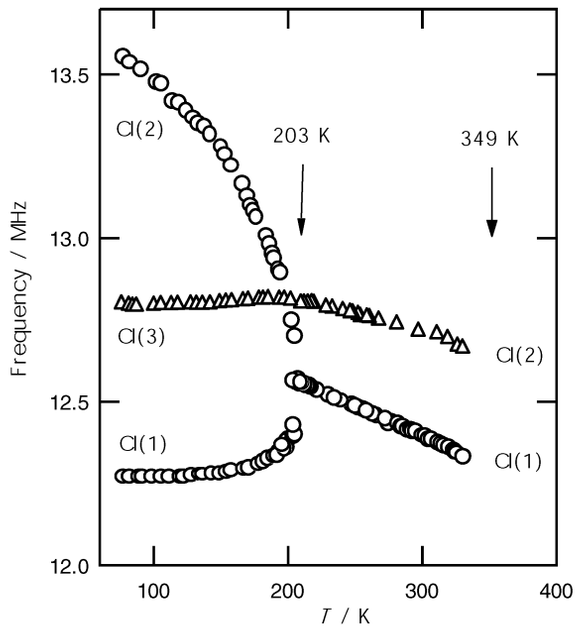

Fig. 2 Temperature dependence of the ^{35}Cl NQR for $CD_3ND_3GeCl_3$. These NQR lines were assigned to three Cl atoms shown in Fig. 7.

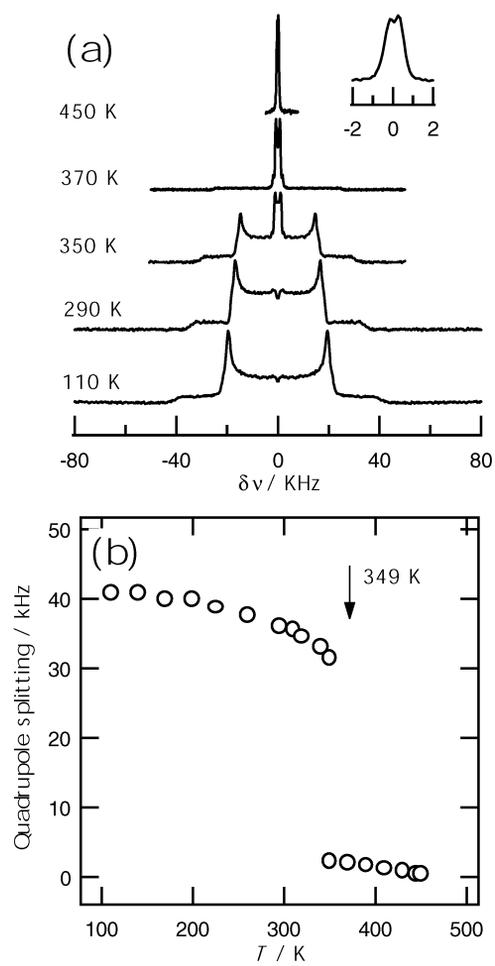

Fig. 3 (a) ^{2}H NMR spectra of $CD_3ND_3GeCl_3$ at selective temperatures. (b) Temperature dependence of the quadrupole splitting.

orientational disorder of the $CD_3ND_3^+$ cation. In accordance with the order–disorder character of this phase transition, a strong endothermic peak on the DTA curve was observed at 349 K, only 3 K lower than that of $CH_3NH_3GeCl_3$. The phase transition to Phase I, however, was not completed during the TOF measurement even at 475 K. For comparison we reexam-

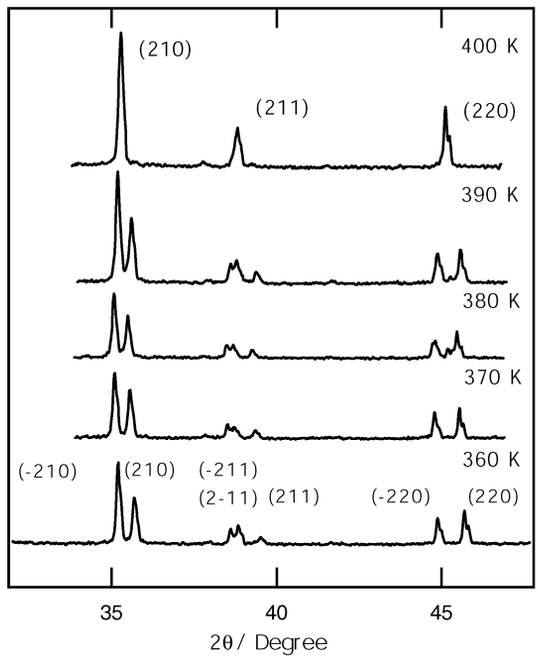

Fig. 4 A part of the XRD powder patterns for $CH_3NH_3GeCl_3$ near T_{tr} (Phase II ↔ I).

ined the corresponding phase transition of $CH_3NH_3GeCl_3$ using a newly prepared sample. Fig. 4 shows XRD patterns with Miller indices over the phase transition region from Phase II to I. In contrast to the deuterated analog, a simple cubic pattern appeared above 400 K consistent with our previous result.[18,19] Furthermore, this strong isotope effect on T_{tr} was also confirmed by the ^2H NMR quadrupole splitting, which was expected to be zero for the cubic phase. Fig. 5 plots the

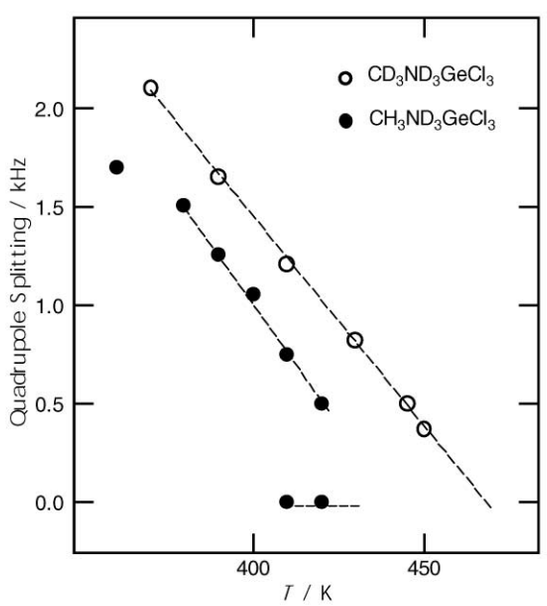

Fig. 5 ^2H NMR quadrupole splittings for $CD_3ND_3GeCl_3$ and $CH_3ND_3GeCl_3$ near the phase transition temperatures from Phase II (trigonal) to I (cubic).

quadrupole splitting against temperature for $CD_3ND_3GeCl_3$ and for N-deuterated $CH_3ND_3GeCl_3$. From these plots we could estimate the phase transition temperatures to be 475 K for $CD_3ND_3GeCl_3$ and 410–420 K for $CH_3ND_3GeCl_3$. It is particularly interesting that this phase transition on the fully deuterated sample is very close to the melting point and almost disappears. On the other hand, the cubic phase of $CH_3NH_3GeCl_3$ was also confirmed by the detection of a sharp ^{14}N NMR signal (FWHM = 2 kHz at 439 K). Since the quadrupole coupling constant (e^2Qq/h) of ^{14}N assigned to a rigid $CH_3NH_3^+$ cation was reported to be 914 kHz at 77 K,[22] the appearance of a sharp ^{14}N NMR signal suggests that the cation is located on an *m*3*m* point symmetry site and that the orientational disorder has a dynamic character.

TOF high-resolution neutron powder diffraction

Table 1 summarizes crystallographic data and experimental details for $CD_3ND_3GeCl_3$ at four different temperatures, 2 K (Phase IV), 250 K (Phase III), 370 K (Phase II), and 475 K (mixture of Phase II and I). Fig. 6(a)–(d) show Rietveld refinement plots for the former time-of-flight windows which correspond to shorter *d*-spacing regions. Final atomic coordinates and selected bond lengths are tabulated in Tables 2 and 3.

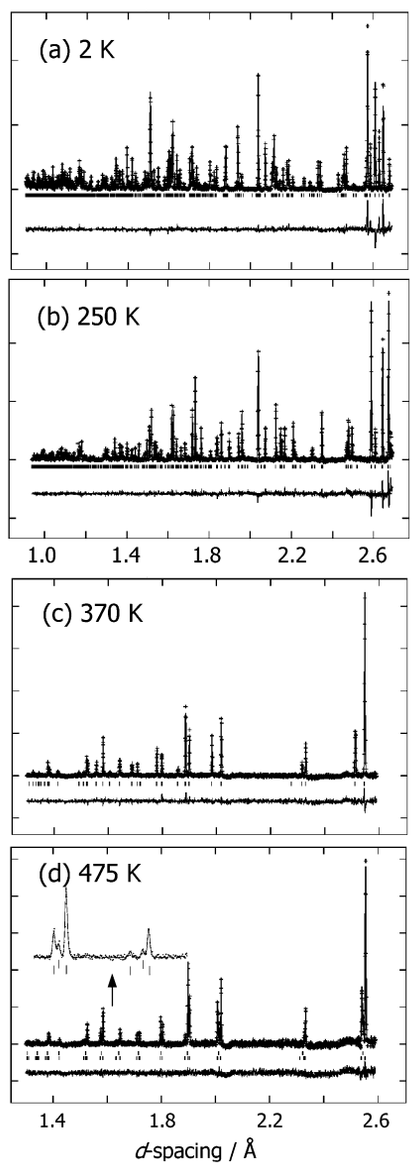

Fig. 6 Final plots of the Rietveld analyses for $CD_3ND_3GeCl_3$. (a) 2 K, (b) 250 K, (c) 370 K and (d) 475 K.

Phase IV. Although the observed powder pattern could be indexed as a monoclinic system, a non-standard setting of the crystal axes was adopted in order to maintain a consistent relation with the high temperature phases. The *a*-axis was chosen as a monoclinic unique axis. At the begining of the refinement for this phase, 19 constraints on the bond lengths

Table 1 Crystallographic data for $CD_3ND_3GeCl_3$ at four different temperatures

Phase	IV	III	II	II	I
Temperature/K	2	250	370	475 (mixture)	
Space group	$P2_1/n$ (No.14)[a]	*Pnma* (No. 62)	*R*3*m* (No.160)	*R*3*m* (No.160)	*Pm*3*m* (No.221)
Crystal system	Monoclinic	Orthorhombic	Trigonal	Trigonal	Cubic
Lattice parameters	a = 10.9973(1) Å b = 7.2043(1) Å c = 8.2911(1) Å α = 90.470(1)°	a = 11.1567(1) Å b = 7.3601(1) Å c = 8.2936(1) Å	a = 5.6584(1) Å α = 90.945(1)°	a = 5.6956(1) Å α = 90.371(1)°	a = 5.6917(2) Å
Z	4	4	1	1	1
D_{calc}/g cm^{-3}	2.195	2.117	1.990	1.951	1.954
R_F	0.0386	0.0820	0.0836	0.0754	0.201
No. of param.[b]	73	92	54	74	
No. of constraints	0	11	15	15	
R_p	0.0567	0.0356	0.0355	0.0321	
R_{wp}	0.0471	0.0329	0.0349	0.0291	
Goodness of fit	2.55	1.93	1.58	1.60	

[a] Unique axis *a*. [b] Profile parameters are not included.

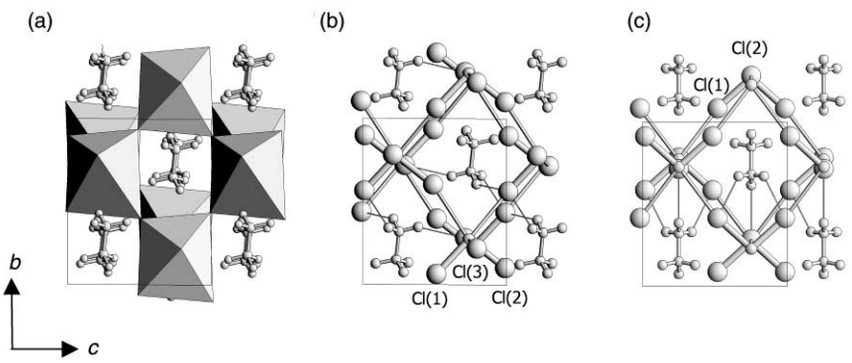

Fig. 7 Crystal structures of $CD_3ND_3GeCl_3$ projected on the *bc* plane. Hydrogen bonds are indicated by lines. (a), (b) show structures of Phase IV at 2 K and (c) shows Phase III at 250 K.

with e.s.d.s = 0.005 Å were introduced for the monomethylammonium cation, they are $d_{C–N}$ = 1.496 Å, three $d_{N–D}$ = 1.025 Å, three $d_{C–D}$ = 1.079 Å [23] and the non-bonding distances including three $d_{N \cdots D(C)}$ = 2.117 Å, three $d_{C \cdots D(C)}$ = 2.077 Å, three $d_{D(C) \cdots D(C)}$ = 1.762 Å and three $d_{D(N) \cdots D(N)}$ = 1.718 Å. These parameters were used for all phases. Under these constraints both CD_3 and ND_3 groups rotate freely keeping an ethane-like structure. At the final refinement all these constraints were released. In the Rietveld refinement process, relatively large thermal parameters were obtained for the D atoms assigned to the ND_3 group compared to the CD_3. This fact suggests the deuteration was not perfect especially on the ND_3 site. Therefore, the structural refinement was performed using a modified scattering length assuming that the substitution is not perfect only on the ND_3 group.

Fig. 7(a) and (b) show the structure at 2 K (Phase IV). Although the perovskite structure is essentially maintained at Phase IV, each $GeCl_6$ octahedral unit is distorted considerably from the regular arrangement and an isolated $GeCl_3^-$ anion can be recognized. Each $GeCl_6$ octahedron has three short bonds (2.365(3), 2.322(3), 2.369(2) Å) and three long bonds (3.187(3), 3.294(3) and 3.197(3) Å) at their *trans* positions, respectively. Three hydrogen bonds, N–D(1) ··· Cl(1), N–D(2) ··· Cl(1) and N–D(3) ··· Cl(3) are recognized but there is no apparent hydrogen bond between Cl(2) and N–D. This geometry of the hydrogen bond is consistent with the ^{35}Cl NQR measurement, in which only one NQR frequency assigned to Cl(2) increases with decreasing temperature as shown in Fig. 3. This fact suggests that Cl(2) is released from the hydrogen bond below 203 K.

Phase III. Since the organic cation is located on the mirror plane, 11 independent constraints on the bond length and the non-bonding distance were introduced throughout the refinements for this phase. As Fig. 7(c) shows, both cation and anion are located on the mirror plane and two hydrogen bonds N–D(2) ··· Cl(1) and N–D(1) ··· Cl(2) are recognized. However, no apparent change was observed in the ^{2}H NMR spectrum at T_{tr} (Phase IV ↔ III), suggesting no drastic change of the cation dynamics. In general, wideline ^{2}H NMR on a powdered sample shows a well known Pake doublet with a splitting, $\Delta\nu_q = (3/4)e^2Qq/h$, where e^2Qq/h is the quadrupole coupling constant at the respective ^{2}H site. Under an axial fast reorientation, the quadrupole splitting reduces to $\Delta\nu_q'$ due to the motional averaging effect and is expressed as,

$$\Delta\nu_q' = \Delta\nu_q(3\cos^2\theta - 1)/2 \qquad (1)$$

where θ is the angle between the principal axis of the electric field gradient (efg) tensor and the rotation axis and $\Delta\nu_q$ is reported to be 120 kHz for rigid CD_3 and ND_3 groups. The observed splitting ($\Delta\nu_q'$) of about 40 kHz in the temperature range from 100 K to 350 K suggests a fast reorientation of the whole cation around the C–N axis because $\cos\theta$ is close to 1/3.

Although reorientation of the cation was much faster than the quadrupole splitting of the rigid lattice, new disordered positions could not be found both for CD_3 and ND_3 groups at Phase III. This fact is also consistent with the DTA measurement in which only a slight base-line shift was observed at T_{tr} (Phase IV ↔ III).

Dynamic structure of the anion in Phases IV and III from ^{35}Cl NQR T_1

The NQR spin–lattice relaxation time (T_1) is very sensitive to slow reorientation containing probe nuclei, since it produces fluctuations of the efg components. The spin–lattice relaxation times (T_1) of the ^{35}Cl NQR were measured using a signal assigned to Cl(1) in the temperature range from 77 K to *ca.* 330

Table 2 Final structural parameters for Phases IV, III, II, and I for $CD_3ND_3GeCl_3$

Phase IV (2 K)[a]

Atom	*x*	*y*	*z*	U_{iso}/Å²
Ge	0.7271(2)	0.2349(4)	0.7742(2)	0.0043(4)
Cl(1)	0.7108(2)	0.0117(3)	0.5645(2)	0.0053(2)
Cl(2)	0.2342(2)	0.0119(3)	−0.1030(2)	0.0048(2)
Cl(3)	0.9418(2)	0.2093(3)	0.7813(2)	0.0037(2)
N	0.0270(2)	0.2484(4)	0.1810(2)	0.0095(4)
C	0.0150(3)	0.7320(5)	0.6482(3)	0.0054(6)
D(1)	0.3965(3)	0.8189(7)	0.6589(4)	0.033(1)
D(2)	0.5389(4)	0.7857(8)	0.6062(4)	0.047(1)
D(3)	0.9540(4)	0.8863(7)	−0.1534(4)	0.038(1)
D(4)	0.0577(3)	0.2191(5)	0.4282(3)	0.025(1)
D(5)	0.0327(2)	0.5900(5)	0.6238(3)	0.028(1)
D(6)	0.5958(2)	0.6888(5)	−0.1317(3)	0.022(1)

Phase III (250 K)

Atom	*x*	*y*	*z*	U_{eq}/Å²
Ge	0.7309(2)	0.25	0.7728(2)	0.015(1)[b]
Cl(1)	0.7225(2)	0.0167(3)	0.5853(2)	0.047(1)
Cl(2)	0.9407(2)	0.25	0.7869(2)	0.038(2)
N	0.5311(2)	0.25	0.3185(1)	0.063(2)
C	0.4887(3)	0.25	0.1473(1)	0.086(2)
D(1)	0.4626(2)	0.25	0.4000(2)	0.23(1)
D(2)	0.5902(2)	0.1482(3)	0.3428(2)	0.22(1)
D(3)	0.5675(2)	0.25	0.0728(2)	0.16(1)
D(4)	0.4385(2)	0.1274(3)	0.1296(2)	0.20(1)

Phase II (370 K)

Atom	*x*	*y*	*z*	Frac.	U_{iso}, U_{eq}/Å²
Ge	0.5	0.5	0.5	1.0	0.03(1)
Cl	0.0938(3)	0.5174(3)	0.5174(3)	1.0	0.10(1)
N	0.2076(2)	0.0265(2)	0.0265(2)	0.3333	0.2[c]
C	−0.0583(2)	0.0358(2)	0.0358(2)	0.3333	0.2
D(1)	0.2700(4)	0.1212(4)	−0.1139(3)	0.1667	0.4
D(2)	0.2626(4)	−0.1451(2)	−0.0073(5)	0.1667	0.4
D(3)	0.2838(3)	0.0966(4)	0.1790(3)	0.1667	0.4
D(4)	−0.1164(4)	0.1656(2)	0.1656(2)	0.3333	0.2
D(5)	−0.1363(2)	−0.1363(2)	0.0726(7)	0.6667	0.2

Phase I (470 K)

Atom	*x*	*y*	*z*	Frac.	U_{iso}/Å²
Ge	0.5	0.5	0.5	1.0	0.02[d]
Cl	0.5	0.5	−0.065(3)	0.5	0.06
N/C	0.076	0.076	0.076	0.25	0.4
D(1)	−0.03	0.184	0.184	0.125	0.4
D(2)	0.040	0.040	0.254	0.125	0.4

[a] Symmetry codes for $P2_1/n$ are (*x, y, z*), (1/2 + *x*, 1/2 − *y*, 1/2 − *z*), (−*x*, −*y*, −*z*), and (1/2 − *x*, 1/2 + *y*, 1/2 + *z*). [b] U_{eq} was defined as 1/3 the trace of the diagonal matrix. [c] Fixed parameters. [d] Fixed parameters.

Table 3 Selected bond distances (Å) and angles (°) in $CD_3ND_3GeCl_3$ for Phase IV (2 K), Phase III (250 K), Phase II (370 K) and Phase I (475 K)

2 K	
trans Cl(1)–Ge–Cl(1)^{I}	2.365(3), 3.187(3)
trans Cl(2)–Ge–Cl(2)^{II}	2.322(3), 3.294(3)
trans Cl(3)–Ge–Cl(3)^{III}	2.369(2), 3.197(3)
Cl(1)–Ge–Cl(2)	94.9(1)
Cl(1)–Ge–Cl(3)	92.4(1)
Cl(2)–Ge–Cl(3)	92.5(1)
N–D(1) ··· Cl(1)	1.017(5), 2.504(5)
< N–D(1) ··· Cl(1)	141.9(3)
N–D(2) ··· Cl(1)	1.001(5), 2.505(5)
< N–D(2) ··· Cl(1)	145.1(3)
N–D(3) ··· Cl(3)	1.023(5), 2.382(5)
< N–D(3) ··· Cl(3)	152.5(3)
250 K	
trans Cl(1)–Ge–Cl(1)^{IV}	2.318(2), 3.294(2)
trans Cl(2)–Ge–Cl(2)^{V}	2.343(2), 3.275(2)
< Cl(1)–Ge–Cl(1)^{VI}	95.6 (1)
< Cl(1)–Ge–Cl(2)	94.2 (1)
370 K	
trans Cl–Ge–Cl	2.31(1), 3.36(1)
< Cl–Ge–Cl	95.6(5)
475 K	
trans Cl–Ge–Cl	2.48 (3), 3.22(3)

I: 1.5 − *x*, 0.5 + *y*, 0.5 + *z*, II: −0.5 + *x*, 0.5 − *y*, 1.5 − *z*, III: 1.5 − *x*, −0.5 + *y*, 0.5 + *z*, IV: 1.5 − *x*, 0.5 + *y*, 0.5 + *z*, V: −0.5 + *x*, 0.5 − *y*, 1.5 − *z*, VI: *x*, 0.5 − *y*, *z*.

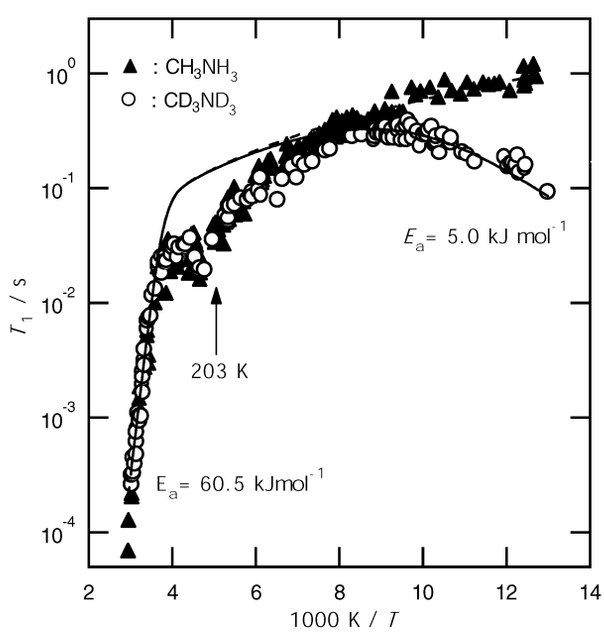

Fig. 8 Spin–lattice relaxation times of the ^{35}Cl NQR are plotted against inverse temperatures for $CH_3NH_3GeCl_3$ and $CD_3ND_3GeCl_3$.

K at which NQR signals disappeared. Fig. 8 plots T_1 against inverse temperature for $CH_3NH_3GeCl_3$ and $CD_3ND_3GeCl_3$. In general NQR relaxation rate ($1/T_1$) is represented by the sum of the following three contributions: Raman processes due to lattice vibrations, reorientation effects of the fragment containing the probe nucleus, and modulation effects of the efg tensor arising from a movable nearby fragment.[24–26] Apart from the anomalous behavior near the phase transition around 203 K, the observed relaxation rates ($1/T_1$) could be expressed using three contributions in units of s^{-1} as,

$$1/T = 1.73\cdot10^{-4}\ s^{-1}\ K^{-2}\cdot T^2 + 1.63\cdot10^{13}\ s^{-1}\cdot\exp(-60.5\ kJ\ mol^{-1}/RT) + (2/3)\omega_Q^{\ 2}(q'/q)^2\tau_c/(1+\tau_c^{\ 2}\omega_Q^{\ 2}), \quad (2)$$

where ω_Q, q'/q and τ_c are the angular NQR frequency, the fraction of the fluctuating efg, and the correlation time of the motion which obeys an Arrhenius relation, respectively. The first and second terms, corresponding to a Raman process and a reorientational motion of the isolated $GeCl_3^-$ anion, are common for both analogs. Therefore, both the orientational disorder of the cation and the reorientation of the $GeCl_3^-$ anion play important roles in the phase transition from Phase III to Phase II.

On the other hand, the T_1 *vs.* $1/T$ plots below 100 K exhibit quite different behaviours between these two analogs, *i.e.*, a modulation effect was observed only for the deuterated analog. Since Cl(1) forms a hydrogen bond with an ND_3 group in Phase

IV, the reorientation of the ND_3 group may modulate the efg at the Cl(1) site. From the best-fit calculation we could estimate $q'/q = 4.6 \times 10^{-3}$ and $\tau_c/s = 4.5 \times 10^{-14} \times \exp(5.0\ kJ\ mol^{-1}/RT)$ for the reorientational correlation time of the ND_3. Our preliminary T_1 results from ^2H NMR also suggested the reorientation of the hole cation around its pseudo C_3 axis. The modulation effect for $CH_3NH_3GeCl_3$ is expected to appear lower than 77 K due to the faster reorientation of the cation.

Structural refinements on Phases II and I

Phase II could be indexed as a trigonal system with space group *R*3*m*. Since our ^2H NMR measurement suggested an almost overall reorientation of the cation, an orientational disorder of the cation was assumed in Phase II. Three C–N orientations related by the trigonal C_3 axis were introduced parallel to the [100], [010] and [001] directions. Rietveld refinement was performed under the 15 constraints on the cation similar to Phase IV or III. Although a slight improvement of the *R* parameters could be achieved accompanied by the further increase of the thermal parameters, these parameters were fixed to the respective values shown in Table 3. This fact suggests that the motional state of the cation is more isotropic than our model. From the final Rietveld refinement, the angle between C–N and the C_3 axis was calculated to be 58.2°. Assuming a three site jump between these orientations the quadrupole splitting of the ^2H NMR was estimated to be 3.3 kHz, which is comparable to the observed splitting (2.1 kHz at 370 K).

An isolated $GeCl_3^-$ anion with a 3*m* symmetry can be recognized and each Ge has three short bonds (Ge–Cl: 2.31(1) Å) and three long bonds (Ge ··· Cl: 3.36(1) Å) at their *trans* positions. This structure is isomorphous with the low temperature forms of $CsGeCl_3$,[14] $CsGeBr_3$, and $CsGeI_3$.[1]

In order to get structural information on Phase I, the furnace temperature was increased to 475 K. However, Phase I could not be obtained as a pure state as shown in Fig. 6(d). From the Rietveld analysis, it became apparent that *ca.* 7% of the sample transformed to a cubic phase. Therefore, the powder pattern could be analyzed as a mixture of two phases; a trigonal phase with space group *R*3*m* and a cubic perovskite phase with space group *Pm*3*m*. Eight different C–N orientations were assumed parallel to the ⟨111⟩ directions for the perovskite phase. The crystal structure of the trigonal phase was essentially same as that at 370 K, however, the structural refinement on the cubic phase revealed a positional disorder of the chloride ion as shown in Fig. 9(b). This characteristic disorder is similar to that

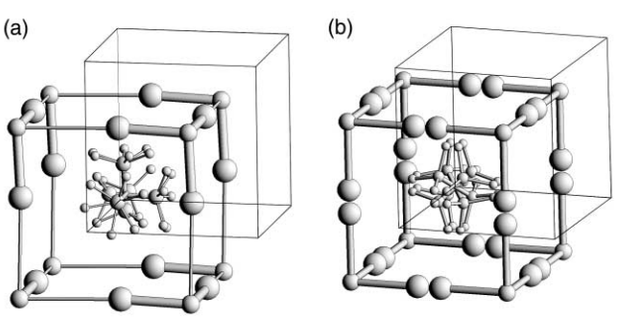

Fig. 9 (a) Crystal structure of Phase II at 370 K. An orientational disorder of the cation appears around the trigonal C_3 axis. (b) Crystal structure of Phase I at 475 K. Only 7% of the sample transformed into this phase. Both orientational disorder of the cation and positional disorder of the chloride ion were introduced into Phase I.

found for $CH_3NH_3GeCl_3$. The Ge–Cl bond length is 2.48(3) Å and the distance between these two disordered sites (6*f* site) is 0.73(3) Å. Since Ge(II) atoms tend to form three short bonds and three longer bonds at their *trans* positions, this disordered structure suggests a dynamic bond switching between Cl–Ge ··· Cl and Cl ··· Ge–Cl.

Correlation between bond lengths for *trans* Cl–Ge ··· Cl

In order to understand the nature of the *trans* Cl–Ge ··· Cl bond, the Ge–Cl bond lengths are plotted against those of the *trans* Ge ··· Cl bond as shown in Fig 10. For comparison a

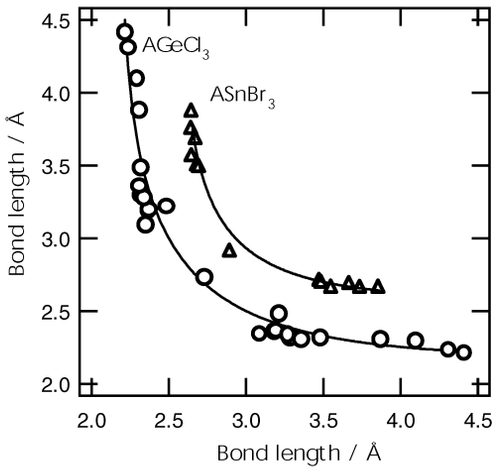

Fig. 10 Correlation between bond lengths for a series of $AGeCl_3$ compounds. Bond length $d_{Ge–Cl}$ is plotted against $d_{Ge\cdots Cl}$ which is located at the *trans* position. For comparison a similar correlation found for $ASnBr_3$ is shown.[15,29]

similar plot for a series of perovskites $ASnBr_3$ (A: Cs and alkylammonium) is also shown. This plot for the $AGeCl_3$ series includes data from $CD_3ND_3GeCl_3$, $RbGeCl_3$,[27] $CsGeCl_3$ [18] and $(CH_3)_4NGeCl_3$.[18] These plots clearly show that the $GeCl_6$ octahedron tends to deform more strongly than the $SnBr_6$ unit and results in the appearance of an isolated anion. The following relation between bond length ($d_{Ge–Cl}$) and bond order (*n*) was assumed similar to the Pauling equation:[15,28]

$$d_{Ge–Cl} = d_0 - a \log(n) \quad (3)$$

where d_0 is a bond length corresponding to $n = 1$ (normal two-center two-electron bond) and *a* is a numerical constant. A symmetric *trans* Cl–Ge–Cl bond can be described as a three-center four-electron (3c–4e) bond in which two electrons occupy the bonding orbital and the remaining two occupy the non-bonding orbital. In this situation the bond order of the Ge–Cl bond can be regarded as $n = 0.5$. Since the number of electrons on the *trans* Cl–Ge–Cl bond remains unchanged upon the asymmetric deformation, the sum of the bond orders of the two *trans* bonds is assumed to be unity. Then, the bond length at the *trans* position can be expressed using a bond order $(1 - n)$ as,[15]

$$d_{Ge\cdots Cl} = d_0 - a \log(1 - n) \quad (4)$$

Eliminating *n* from eqn. (3) and (4), the best-fit parameters d_0 and *a* were determined to be 2.18(1) Å and 1.69(1) Å, respectively. The solid lines in Fig. 10 show the calculated correlation between $d_{Ge–Cl}$ and $d_{Ge\cdots Cl}$ using these parameters.

Ionic conductivity of $CD_3ND_3GeCl_3$

Fig. 11 shows the temperature dependence of the conductivity for $CD_3ND_3GeCl_3$ together with the previously reported data for $CH_3NH_3GeCl_3$.[18,19] In contrast to $CH_3NH_3GeCl_3$, a steep increase of the conductivity could not be observed for $CD_3ND_3GeCl_3$ just below T_{tr} (Phase II ↔ I). This is not surprising because the cubic phase of the deuterated analog appears about 80 K higher than that in $CH_3NH_3GeCl_3$. Although the high-conducting cubic phase of $CD_3ND_3GeCl_3$ could not be obtained as a pure state, the conducting mech-

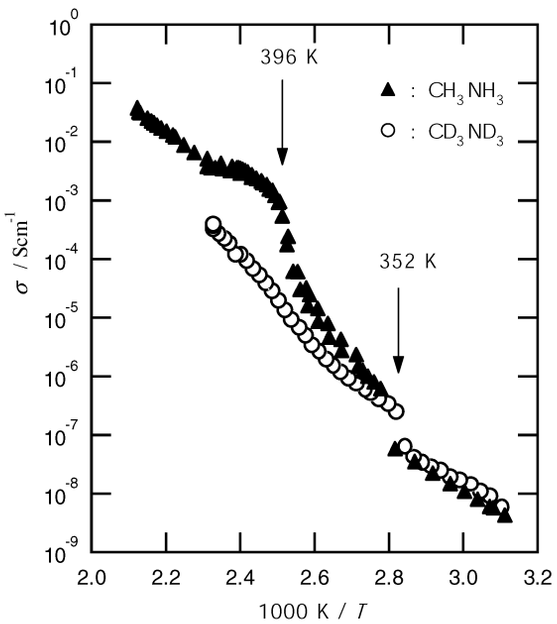

Fig. 11 Ionic conductivity against inverse temperature for $CD_3ND_3GeCl_3$ and $CH_3NH_3GeCl_3$. Arrows indicate T_{tr} (Phase III ↔ II) and T_{tr} (Phase II ↔ I) for $CH_3NH_3GeCl_3$.

anism reported for $CH_3NH_3GeCl_3$ was confirmed to be correct. That is, the positional disorder of the chloride ion together with the reorientation of the $GeCl_3^-$ anion plays an important role in the conduction of the chloride ion. However, the essential reason for the strong isotope effect on T_{tr} (Phase II ↔ I) and a possibility of ferroelectricity are still interesting subjects.

Acknowledgements

This work was supported by a Grant-in-Aid for Scientific Research No.11694084 from the Ministry of Education, Science, Sports and Culture, Japan.

References

1 G. Thiele, H. W. Rotter and K. D. Schmidt, *Z. Anorg. Allg. Chem.*, 1987, **545**, 148.
2 G. Thiele, H. W. Rotter and K. D. Schmidt, *Z. Anorg. Allg. Chem.*, 1988, **559**, 7.
3 W. Depmeier and A. Möller, *Acta Crystallogr., Sect. B*, 1980, **36**, 803.
4 K. Yamada, S. Nose, T. Umehara, T. Okuda and S. Ichiba, *Bull. Chem. Soc. Jpn.*, 1988, **61**, 4265.
5 K. Yamada, S. Funabiki, H. Horimoto, T. Matsui, T. Okuda and S. Ichiba, *Chem. Lett.*, 1991, 801.
6 S. Plesko, R. Kind and J. Roos, *J. Phys. Soc. Jpn.*, 1978, **45**, 553.
7 S. Sharma, N. Weiden and A. Weiss, *Z. Naturforsch., Teil A*, 1991, **46**, 329.
8 A. Poglitsch and D. Weber, *J. Chem. Phys.*, 1987, **87**, 6373.
9 K. Yamada, T. Matsui, T. Tsuritani, T. Okuda and S. Ichiba, *Z. Naturforsch., Teil A*, 1990, **45**, 307.
10 K. Yamada, H. Kawaguchi, T. Matsui, T. Okuda and S. Ichiba, *Bull. Chem. Soc. Jpn.*, 1990, **63**, 2521.
11 N. Onoda-Yamamuro, T. Matsuo and H. Suga, *J. Chem. Thermodynam.*, 1991, **23**, 987.
12 K. Yamada, Y. Kuranaga, K. Ueda, S. Goto, T. Okuda and Y. Furukawa, *Bull. Chem. Soc. Jpn.*, 1998, **71**, 127.
13 D. K. Seo, N. Gupta, M.-H. Whangbo, M. Hillebrecht and G. Thiele, *Inorg. Chem.*, 1998, **37**, 407.
14 A. N. Christensen and S. E. Rasmussen, *Acta Chem. Scand.*, 1965, **19**, 421.
15 K. Yamada and T. Okuda, in *Chemistry of Hypervalent Compounds*, ed. K. Akiba, Wiley-VCH, New York, 1999, ch. 3.
16 G. C. Pimentel and R. D. Spratley, *Chemical Bonding*, Holden-Day, Inc., San Francisco, 1969, ch. 7.
17 K. Yamada, T. Tsuda, C. Holst, T. Okuda, H. Ehrenberg, I. Svoboda, H.-G. Krane and H. Fuess, *Bull. Chem. Soc. Jpn.*, 2001, **74**, 77.
18 K. Yamada, K. Isobe, T. Okuda and Y. Furukawa, *Z. Naturforsch., Teil A*, 1994, **49**, 258.
19 K. Yamada, K. Isobe, E. Tsuyama, T. Okuda and Y. Furukawa, *Solid State Ionics*, 1995, **79**, 152.
20 T. Okuda, S. Gotou, T. Takahashi, H. Terao and K. Yamada, *Z. Naturforsch., Teil A*, 1996, **51**, 686.
21 A. C. Larson and R. B. Von Dreele, GSAS, LAUR 86–748, Los Alamos National Laboratory, Los Alamos, NM, 2000.
22 M. J. Hunt and A. L. Mackay, *J. Magn. Reson.*, 1974, **15**, 402.
23 V. Rodriguez, G. Aguirre-Zamalloa, M. Couzi and T. Roisnel, *J. Phys. Condens. Matter*, 1996, **8**, 969.
24 H. Chihara and N. Nakamura, in *Advances in Nuclear Quadrupole Resonance*, vol. 4, ed. J. A. S. Smith, Heyden & Son Ltd., London, 1980, p. 1.
25 T. Asaji and T. Ishizaka, *Z. Naturforsch., Teil A*, 2000, **55**, 83.
26 K. Yamada, M. Kinoshita, K. Hosokawa and T. Okuda, *Bull. Chem. Soc. Jpn.*, 1993, **66**, 1317.
27 D. Messer, *Z. Naturforsch., Teil B*, 1978, **33**, 366.
28 L. Pauling, *The Nature of the Chemical Bond*, Cornell University Press, New York, 1960, ch. 7.
29 G. Thiele and B. R. Serr, *Z. Kristallogr.*, 1996, **211**, 46; G. Thiele and B. R. Serr, *Z. Kristallogr.*, 1996, **211**, 47.